CAUCHY – Jurnal Matematika Murni dan Aplikasi
Volume 11 (1) (2026), Pages 540-555
p-ISSN: 2086-0382; e-ISSN: 2477-3344

Stability and Bifurcation of a 3D Eco Epidemiological Predator Prey Model with Pesticide

Aqiilah Ollyana Savitri and Dian Savitri*

Department of Mathematics, Universitas Negeri Surabaya, Indonesia

Abstract

Eco–epidemiological predator–prey models provide an important mathematical framework for understanding the interaction between disease transmission, predation, and human intervention in ecological systems. This study investigates a three–dimensional deterministic model incorporating saturated disease incidence, Holling type II predation, and pesticide application. Analytical techniques are employed to determine the existence and local stability of biologically feasible equilibrium points, while numerical simulations using a fourth–order Runge–Kutta method illustrate the dynamical behavior of the system under different parameter regimes. The analysis reveals the possibility of disease–free, predator–free, and interior coexistence equilibria, as well as bistability depending on parameter values and initial conditions. Bifurcation analysis identifies critical thresholds in disease transmission and predator conversion efficiency that govern transitions between predator persistence and extinction. These findings provide theoretical insights for integrated pest management strategies by emphasizing the balance between chemical control and ecological stability.

Keywords: bifurcation; eco-epidemiological model; pesticide effect; predator–prey system; stability

1. Introduction

Eco-epidemiological predator–prey models provide a fundamental mathematical framework for understanding the interaction between population dynamics and infectious disease transmission in ecological systems [1], [2]. Such models are widely employed to study population regulation, biodiversity maintenance, and integrated pest management under simultaneous ecological and epidemiological influences [3], [4]. Their relevance has increased in recent years due to growing concerns regarding wildlife diseases and sustainable agricultural control strategies.

Recent developments in eco-epidemic modeling include deterministic, stochastic, and fractional-order formulations, revealing rich dynamical behaviors such as coexistence equilibria, periodic oscillations, bifurcations, and extinction scenarios [5], [6]. Incorporating behavioral mechanisms—including fear effects [7], [8], herding behavior [9], hunting cooperation [10], [11], and time delays [12]—has significantly deepened understanding of how adaptive ecological responses interact with disease transmission. Additional structural complexity arises from competitive interactions and shared-resource mechanisms [13].

*Corresponding author. E-mail: diansavitri@unesa.ac.id

Submitted: January 24, 2026 Reviewed: February 06, 2026 Accepted: March 03, 2026
DOI: https://doi.org/10.18860/cauchy.v11i1.40676

From an applied standpoint, eco-epidemiological models are instrumental in designing effective pest and disease management policies. Various studies have incorporated harvesting strategies, pesticide applications, isolation mechanisms, and optimal control formulations to suppress infection while preserving ecological balance [14], [15], [16], [17]. More advanced approaches, including backstepping control [18], impulsive interventions, and reaction–diffusion systems [19], [20], further enhance stabilization and spatial realism. Investigations of pathogen-avoidance behavior in predator–prey–scavenger systems have also provided additional ecological insight [21].

Despite these advances, relatively limited attention has been given to analyzing a minimal deterministic eco-epidemiological framework that simultaneously incorporates three essential biological mechanisms within a unified three-dimensional ordinary differential equation system: saturated disease incidence, Holling type II functional response, and pesticide intervention effects [22], [23]. Many existing models emphasize either sophisticated control techniques or higher-order dynamics, whereas a systematic analytical investigation of their combined interaction remains comparatively underexplored.

Motivated by this gap, the present study develops and analyzes a predator–prey eco-epidemiological model that integrates infected prey dynamics with pesticide intervention. The objectives are threefold. First, we formulate a biologically consistent model incorporating saturated incidence, Holling type II predation, and pesticide-induced mortality. Second, we investigate the existence and feasibility conditions of equilibria and analyze their local stability properties. Third, we complement the analytical results with numerical simulations to illustrate the qualitative behavior of the system and explore parameter-dependent dynamical transitions.

Biologically, pesticide application is assumed to act primarily on susceptible prey, reflecting common agricultural practices in which chemical agents target pest populations rather than higher trophic levels. While non-target effects may occur in real ecosystems, this simplifying assumption enables clearer analytical interpretation of how chemical control influences disease transmission and predator persistence. The implications of this assumption are discussed as a possible extension for future work.

Compared with related models, the present framework combines structural elements that are typically studied separately. The model in [22] considers competitive predator dynamics without pesticide intervention, whereas [23] investigates stability and Hopf bifurcation properties but employs standard bilinear incidence and omits explicit chemical control. In contrast, this study integrates saturated incidence, Holling type II predation, and pesticide-induced mortality within a single deterministic system. The simultaneous interaction of these mechanisms modifies the equilibrium structure and stability conditions, potentially leading to threshold behavior and stability transitions that differ from previously reported results.

The remainder of this paper is organized as follows. Section 2 presents the mathematical formulation and analytical framework. Section 3 provides the equilibrium analysis, local stability investigation, and supporting numerical simulations. Section 4 summarizes the main findings and outlines directions for future research.

2. Methods

This study employs a theoretical and computational framework based on nonlinear dynamical systems to investigate the interactions among susceptible prey, infected prey, and predators under pesticide intervention. The methodological approach integrates qualitative analysis, local stability theory, and numerical simulations to explore equilibrium structure, stability properties, and bifurcation behavior.

2.1. Study Design and Model Formulation

The model consists of three interacting populations: susceptible prey $S(t)$, infected prey $I(t)$, and predators $P(t)$. The formulation is based on biologically motivated assumptions consistent

with established eco-epidemiological theory [4], [5].

Susceptible prey are assumed to grow logistically with intrinsic growth rate r and environmental carrying capacity K. Both susceptible and infected prey compete for the same limited resources. Disease transmission follows a saturated incidence function $\frac{\beta SI}{1+I}$, where β denotes the transmission coefficient. The saturation term $(1+I)^{-1}$ accounts for reduced effective contact at high infection levels and avoids unbounded growth typical of bilinear incidence.

Predation dynamics incorporate distinct functional responses to reflect differential vulnerability between healthy and infected prey. Consumption of susceptible prey follows a Holling type II functional response $\frac{mS}{h+S}$, where m is the predation rate and h is the half-saturation constant, reflecting predator handling time. Infected prey, due to their weakened condition, are consumed via a linear term nI, representing the assumption that they are captured with negligible handling time. This mixed functional response has been widely adopted in eco-epidemiological models to capture the increased susceptibility of infected prey.

Pesticide application is modeled as an additional mortality term uS acting only on susceptible prey. Predation contributes to predator recruitment through conversion efficiencies η (from susceptible prey) and α (from infected prey). Since the model is formulated at the population level, η and α are not restricted to values below unity. Natural predator mortality is represented by μ, while infected prey experience disease-induced mortality at the rate ρ.

Under these assumptions, the system is given by:

$$\frac{dS}{dt} = rS\left(1 - \frac{S+I}{K}\right) - \frac{\beta SI}{1+I} - \frac{mSP}{h+S} - uS, \tag{1}$$

$$\frac{dI}{dt} = \frac{\beta SI}{1+I} - nIP - \rho I, \tag{2}$$

$$\frac{dP}{dt} = \frac{\eta mSP}{h+S} + \alpha nIP - \mu P. \tag{3}$$

All parameters are assumed to be positive constants. Their biological interpretations are summarized in Table 1.

Table 1: Biological interpretation of model parameters

Parameter	Definition
r	Intrinsic growth rate of prey
K	Environmental carrying capacity
β	Disease transmission rate
ρ	Disease-induced mortality rate
m	Predation rate on susceptible prey
n	Predation rate on infected prey
h	Half-saturation constant
η	Predator recruitment efficiency from susceptible prey
α	Predator recruitment efficiency from infected prey
μ	Natural predator mortality
u	Pesticide application rate

2.2. Analytical Framework

Equilibrium points are obtained by solving the steady-state system

$$\frac{dS}{dt} = \frac{dI}{dt} = \frac{dP}{dt} = 0.$$

The biologically relevant equilibria include:

$$E_0 = (0,0,0), \quad E_1 = (S_1,0,0), \quad E_2 = (S_2,0,P_2), \quad E_3 = (S_3,I_3,0), \quad E^* = (S^*,I^*,P^*).$$

The disease-free equilibrium E_1 exists provided $r > u$, ensuring $S_1 = \frac{K(r-u)}{r} > 0$. The existence of E_2 and E_3 requires positivity of their respective components, leading to parameter constraints derived explicitly in Section 3. The interior equilibrium E^* exists when $S^* > 0$, $I^* > 0$, and $P^* > 0$.

2.2.1. Basic Reproduction Numbers

The basic reproduction number of the disease is computed using the next-generation matrix method and is given by

$$\mathcal{R}_0 = \frac{\beta S_1}{\rho} = \frac{\beta K(r-u)}{r\rho}.$$

The endemic equilibrium E_3 may exist only when $\mathcal{R}_0 > 1$. Similarly, the predator invasion threshold is defined as

$$\mathcal{R}_p = \frac{\eta m S_1}{\mu(h+S_1)},$$

which determines whether predators can invade the disease-free equilibrium.

2.2.2. Local Stability Analysis

Local stability is determined by linearizing system Eqs. (1)–(3) around each equilibrium. The Jacobian matrix is

$$J(S,I,P) = \begin{pmatrix} a_{11} & a_{12} & a_{13} \\ a_{21} & a_{22} & a_{23} \\ a_{31} & a_{32} & a_{33} \end{pmatrix},$$

where

$$\begin{aligned}
a_{11} &= r\left(1 - \frac{2S+I}{K}\right) - \frac{\beta I}{1+I} - \frac{mPh}{(h+S)^2} - u, \\
a_{12} &= -\frac{rS}{K} - \frac{\beta S}{(1+I)^2}, \\
a_{13} &= -\frac{mS}{h+S}, \\
a_{21} &= \frac{\beta I}{1+I}, \\
a_{22} &= \frac{\beta S}{(1+I)^2} - nP - \rho, \\
a_{23} &= -nI, \\
a_{31} &= \frac{\eta m P h}{(h+S)^2}, \\
a_{32} &= \alpha n P, \\
a_{33} &= \frac{\eta m S}{h+S} + \alpha n I - \mu.
\end{aligned}$$

For boundary equilibria, stability is determined from eigenvalues directly. For the interior equilibrium, the characteristic polynomial is cubic, and stability is established using the Routh–Hurwitz criteria.

2.3. Numerical and Computational Procedures

All symbolic computations and numerical simulations are performed using Maple 2023 [24]. Numerical integration is conducted using the classical fourth-order Runge–Kutta (RK4) scheme with fixed step size $\Delta t = 0.01$, which is sufficiently small to ensure numerical accuracy and convergence.

Sensitivity analysis is carried out using one-parameter variation while holding other parameters fixed, allowing identification of thresholds influencing qualitative system behavior [25]. Bifurcation diagrams are generated via numerical continuation by varying selected parameters, particularly the disease transmission rate β and predator conversion efficiency η, to detect stability switching and qualitative transitions in long-term dynamics.

3. Results and Discussion

This section presents the main analytical and numerical findings of the proposed eco–epidemiological model. We first derive the biologically feasible equilibrium points and their existence conditions, then examine local stability via the Jacobian and Routh–Hurwitz criteria. Finally, numerical simulations and bifurcation diagrams are provided to illustrate stability transitions and parameter thresholds that characterize disease persistence and predator survival under pesticide intervention.

3.1. Equilibrium Analysis

Equilibrium points of system Eqs. (1)–(3) are obtained by solving

$$\frac{dS}{dt} = 0, \quad \frac{dI}{dt} = 0, \quad \frac{dP}{dt} = 0.$$

Using symbolic computation in Maple 2023, the model admits several biologically relevant equilibrium points.

1. Trivial equilibrium. The point $E_0 = (0, 0, 0)$ represents the extinction of all populations.
2. Disease-free and predator-free equilibrium.

   $$E_1 = \left(\frac{K(r-u)}{r},\, 0,\, 0\right),$$

   which exists provided $r > u$. Biologically, this condition ensures that the intrinsic growth rate of prey exceeds pesticide-induced mortality.
3. Predator–prey equilibrium without infection.

   $$E_2 = (S_2, 0, P_2) = \left(\frac{\mu h}{\eta m - \mu},\, 0,\, \frac{h\eta\left(\eta K m(r-u) - \mu(hr + K(r-u))\right)}{(\eta m - \mu)^2 K}\right).$$

   This equilibrium exists if the following feasibility conditions hold:

   $$\eta m > \mu, \tag{4}$$
   $$\eta K m(r-u) > \mu\left(hr + K(r-u)\right). \tag{5}$$

   Condition in Eq. (4) guarantees $S_2 > 0$, while Eq. (5) ensures $P_2 > 0$.
4. Predator-free endemic equilibrium E_3. Setting $P = 0$ and $I > 0$, the third equation is automatically satisfied. From the infected equation

   $$\frac{\beta S I}{1+I} - \rho I = 0,$$

   and since $I > 0$, we obtain

   $$\frac{\beta S}{1+I} = \rho \quad \Longrightarrow \quad S = \frac{\rho(1+I)}{\beta}. \tag{6}$$

   Substituting Eq. (6) into the susceptible equation

   $$rS\left(1 - \frac{S+I}{K}\right) - \frac{\beta S I}{1+I} - uS = 0,$$

and simplifying algebraically yields a quadratic equation in I:

$$AI^2 + BI + C = 0, \tag{7}$$

where the coefficients are given by

$$A = \frac{r\rho}{K\beta} > 0,$$

$$B = \frac{r\rho}{K\beta} + \frac{r\rho}{\beta} - \frac{r\rho^2}{K\beta^2} - \frac{\rho}{\beta}(r-u),$$

$$C = \frac{r\rho}{\beta} - \frac{r\rho^2}{K\beta^2} - \frac{\rho}{\beta}(r-u).$$

The discriminant of Eq. (7) is $\Delta = B^2 - 4AC$. Since $A > 0$ (all parameters are positive), the quadratic opens upward and the biologically feasible endemic equilibrium corresponds to the positive root

$$I_3 = \frac{-B + \sqrt{\Delta}}{2A},$$

which is real and positive provided $\Delta > 0$ and $-B + \sqrt{\Delta} > 0$. Once I_3 is determined, the corresponding susceptible component follows from Eq. (6):

$$S_3 = \frac{\rho(1+I_3)}{\beta},$$

which is automatically positive whenever $I_3 > 0$. The predator-free endemic equilibrium is therefore given by $E_3 = (S_3, I_3, 0)$. These analytical existence conditions are further illustrated numerically in the simulations presented in the following subsections.

5. Interior (coexistence) equilibrium.

$$E^* = (S^*, I^*, P^*)$$

is obtained by solving the full nonlinear algebraic system. Due to algebraic complexity, the explicit expressions are omitted here but computed symbolically in Maple. Feasibility requires $S^* > 0$, $I^* > 0$, and $P^* > 0$. Each equilibrium corresponds to a distinct ecological regime. Their existence depends on biologically meaningful parameter restrictions, particularly those governing disease transmission, predator conversion efficiency, and pesticide intensity. These feasibility conditions provide the foundation for the stability and bifurcation analysis presented in the subsequent subsections.

3.2. Stability Analysis

The local stability of each equilibrium point is determined by evaluating the Jacobian matrix of system Eqs. (1)–(3) at the corresponding equilibrium and analyzing the signs of its eigenvalues. The Jacobian matrix of system Eqs. (1)–(3) is given by

$$J(S,I,P) = \begin{pmatrix} r\left(1 - \frac{2S+I}{K}\right) - \frac{\beta I}{1+I} - \frac{mPh}{(h+S)^2} - u & -\frac{rS}{K} - \frac{\beta S}{(1+I)^2} & -\frac{mS}{h+S} \\ \frac{\beta I}{1+I} & \frac{\beta S}{(1+I)^2} - nP - \rho & -nI \\ \frac{\eta mPh}{(h+S)^2} & \alpha nP & \frac{\eta mS}{h+S} + \alpha nI - \mu \end{pmatrix}.$$

Theorem 3.1. *The trivial equilibrium $E_0 = (0,0,0)$ is unstable.*

Proof. Evaluating the Jacobian matrix at E_0 yields

$$J(E_0) = \begin{pmatrix} r-u & 0 & 0 \\ 0 & -\rho & 0 \\ 0 & 0 & -\mu \end{pmatrix}.$$

The eigenvalues are $\lambda_1 = r - u$, $\lambda_2 = -\rho$, and $\lambda_3 = -\mu$. Since $r > u$ under biologically realistic assumptions, we have $\lambda_1 > 0$, while $\lambda_2 < 0$ and $\lambda_3 < 0$. Hence, E_0 is unstable. □

Theorem 3.2. *The disease-free equilibrium*

$$E_1 = \left(\frac{K(r-u)}{r}, 0, 0\right)$$

is locally asymptotically stable if

$$\mathcal{R}_0 < 1 \quad \textit{and} \quad \frac{\eta m K(r-u)}{hr + K(r-u)} < \mu,$$

where

$$\mathcal{R}_0 = \frac{\beta S_1}{\rho}, \qquad S_1 = \frac{K(r-u)}{r}.$$

Proof. Evaluating the Jacobian matrix at E_1 yields

$$J(E_1) = \begin{pmatrix} -(r-u) & -\beta S_1 & -\dfrac{mS_1}{h+S_1} \\ 0 & \beta S_1 - \rho & 0 \\ 0 & 0 & \dfrac{\eta m S_1}{h+S_1} - \mu \end{pmatrix}.$$

Since the matrix is upper triangular, its eigenvalues are given directly by the diagonal entries:

$$\lambda_1 = -(r-u), \quad \lambda_2 = \beta S_1 - \rho, \quad \lambda_3 = \frac{\eta m S_1}{h+S_1} - \mu.$$

Clearly, $\lambda_1 < 0$ whenever $r > u$, which is the existence condition for E_1.
For the second eigenvalue, we rewrite it as

$$\lambda_2 = \rho\left(\frac{\beta S_1}{\rho} - 1\right) = \rho(\mathcal{R}_0 - 1).$$

Thus, $\lambda_2 < 0$ if and only if $\mathcal{R}_0 < 1$.
For the third eigenvalue, $\lambda_3 < 0$ is equivalent to

$$\frac{\eta m S_1}{h+S_1} < \mu.$$

Substituting $S_1 = \frac{K(r-u)}{r}$ and simplifying yields

$$\frac{\eta m K(r-u)}{hr + K(r-u)} < \mu.$$

Therefore, all eigenvalues have negative real parts under the stated conditions, and the equilibrium E_1 is locally asymptotically stable. □

Theorem 3.3. *The predator–prey equilibrium without infection $E_2 = (S_2, 0, P_2)$ is locally asymptotically stable if*

$$\beta S_2 - nP_2 - \rho < 0$$

and the Routh–Hurwitz conditions for the prey–predator subsystem are satisfied.

Proof. Evaluating the Jacobian at E_2 yields

$$J(E_2) = \begin{pmatrix} a_{11} & -\dfrac{rS_2}{K} - \beta S_2 & -\dfrac{mS_2}{h+S_2} \\ 0 & \beta S_2 - nP_2 - \rho & 0 \\ a_{31} & \alpha n P_2 & a_{33} \end{pmatrix},$$

where

$$a_{11} = r\left(1 - \frac{2S_2}{K}\right) - \frac{mP_2 h}{(h+S_2)^2} - u, \quad a_{31} = \frac{\eta m P_2 h}{(h+S_2)^2}, \quad a_{33} = \frac{\eta m S_2}{h+S_2} - \mu.$$

Since the Jacobian has a block-triangular structure, one eigenvalue is

$$\lambda_1 = \beta S_2 - nP_2 - \rho.$$

The remaining eigenvalues are determined by the 2×2 subsystem

$$J_{SP}(E_2) = \begin{pmatrix} a_{11} & -\dfrac{mS_2}{h+S_2} \\ a_{31} & a_{33} \end{pmatrix}.$$

Its characteristic polynomial is

$$\lambda^2 + b_1 \lambda + b_2 = 0,$$

where

$$b_1 = -(a_{11} + a_{33}), \qquad b_2 = a_{11}a_{33} + \frac{mS_2}{h+S_2} a_{31}.$$

According to the Routh–Hurwitz criterion for second-order systems, the subsystem is locally asymptotically stable if and only if

$$b_1 > 0 \quad \text{and} \quad b_2 > 0.$$

This completes the proof. □

Theorem 3.4. *The predator-free endemic equilibrium $E_3 = (S_3, I_3, 0)$ is locally asymptotically stable if*

$$\frac{\eta m S_3}{h+S_3} + \alpha n I_3 < \mu$$

and the Routh–Hurwitz conditions for the disease subsystem are satisfied.

Proof. Evaluating the Jacobian at E_3 gives

$$J(E_3) = \begin{pmatrix} a_{11} & a_{12} & -\dfrac{mS_3}{h+S_3} \\ a_{21} & a_{22} & -nI_3 \\ 0 & 0 & \dfrac{\eta m S_3}{h+S_3} + \alpha n I_3 - \mu \end{pmatrix}.$$

Since the matrix is block triangular, one eigenvalue is

$$\lambda_1 = \frac{\eta m S_3}{h + S_3} + \alpha n I_3 - \mu.$$

The remaining eigenvalues are determined by the disease subsystem

$$J_{SI}(E_3) = \begin{pmatrix} a_{11} & a_{12} \\ a_{21} & a_{22} \end{pmatrix}.$$

Its characteristic polynomial is

$$\lambda^2 + d_1\lambda + d_2 = 0,$$

where

$$d_1 = -(a_{11} + a_{22}), \qquad d_2 = a_{11}a_{22} - a_{12}a_{21}.$$

The subsystem is locally asymptotically stable if and only if

$$d_1 > 0 \quad \text{and} \quad d_2 > 0.$$

Thus, E_3 is locally asymptotically stable if predators cannot invade ($\lambda_1 < 0$) and the disease subsystem satisfies the Routh–Hurwitz conditions. □

Theorem 3.5. *The interior equilibrium $E^* = (S^*, I^*, P^*)$ is locally asymptotically stable if the Routh–Hurwitz conditions for the cubic characteristic polynomial of $J(E^*)$ are satisfied.*

Proof. The characteristic equation of $J(E^*)$ is

$$\lambda^3 + c_1\lambda^2 + c_2\lambda + c_3 = 0,$$

where

$$c_1 = -\operatorname{tr}(J(E^*)), \quad c_2 = \text{sum of principal second-order minors}, \quad c_3 = -\det(J(E^*)).$$

According to the Routh–Hurwitz criterion for third-order polynomials, E^* is locally asymptotically stable if and only if

$$c_1 > 0, \quad c_2 > 0, \quad c_3 > 0, \quad c_1c_2 > c_3.$$

Due to the algebraic complexity of the coefficients, these conditions are verified numerically in the subsequent section. □

3.3. Numerical Simulations

Numerical simulations were carried out using the classical fourth-order Runge–Kutta (RK4) method implemented in Maple 2023. All simulations were performed on the time interval $t \in [0, 200]$ using a fixed step size $\Delta t = 0.01$. Additional computations with smaller step sizes produced identical qualitative behavior, confirming numerical consistency.

The parameter values used in the simulations are summarized in Table 2. These values are selected from biologically plausible ranges reported in the literature [3], [22] to illustrate the qualitative dynamical behavior of the system, rather than to represent a specific field scenario. Additional simulations (not shown) indicate that moderate variations in the pesticide application rate u do not alter the qualitative dynamics, suggesting robustness of the results.

For clarity in graphical illustrations, the numerically computed equilibria corresponding to

different parameter regimes are denoted by E_6 and E_7. The complete parameter set for each case is specified in the respective figure caption to ensure reproducibility.

Table 2: Parameter values used in numerical simulations

Parameter	Value	Reference
r	0.7 (Case 1), 9.7 (Cases 2, 3)	[3] and Assumed
β	0.7	Assumed
μ	0.6 (Case 1), 0.063 (Case 2), 0.63 (Case 3)	Assumed
η	4.26263 (Case 1), 0.26263 (Case 2), 3.26263 (Case 3)	Assumed
u	0.05 (Case 1), 0.5 (Cases 2, 3)	Assumed
h	2.1	Assumed
K	0.64	Assumed
ρ	0.047	Assumed
α	0.02 (Case 1), 0.2 (Cases 2, 3)	Assumed
m	1.3 (Case 1), 0.4 (Case 2), 1.4 (Case 3)	Assumed
n	1.3 (Case 1), 1.1 (Cases 2, 3)	Assumed

3.3.1. Stability of equilibrium E_6 (Case 1)

For the parameter set in Case 1, the system admits a predator–prey equilibrium without infection,

$$E_6 = (0.255, 0, 0.672).$$

The Jacobian matrix evaluated at E_6 has eigenvalues

$$-0.119 \pm 0.429i, \quad -0.742,$$

whose negative real parts confirm local asymptotic stability.

Fig. 1 shows trajectories originating from $N_1(0.4, 0.05, 0.9)$ and $N_2(0.35, 0.02, 0.80)$, both converging to E_6. The infected prey component vanishes asymptotically, while the susceptible prey and predator populations stabilize at positive levels. These numerical findings are fully consistent with the analytical stability conditions derived in the previous section.

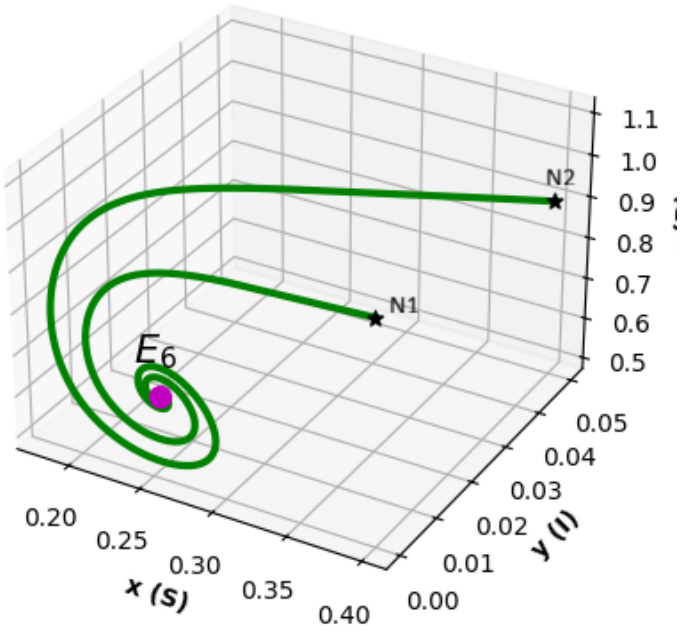

Fig. 1: Phase portrait illustrating convergence to the stable equilibrium $E_6(0.255, 0, 0.672)$ under Case 1 parameters.

3.3.2. Stability of equilibrium E_7 (Case 1)

Under the parameter regime of Case 2, the system possesses a positive interior coexistence equilibrium,

$$E_7 = (0.385, 0.212, 0.159).$$

The eigenvalues of the Jacobian at E_7 are

$$-5.698, \quad -0.098, \quad -0.072,$$

which are all negative, establishing local asymptotic stability.

Fig. 2 illustrates convergence from distinct initial conditions $N_3(0.3, 0.23, 0.15)$, $N_4(0.35, 0.2, 0.16)$, and $N_5(0.4, 0.25, 0.1)$ toward E_7. The long-term coexistence of susceptible prey, infected prey, and predator populations confirms the theoretical predictions.

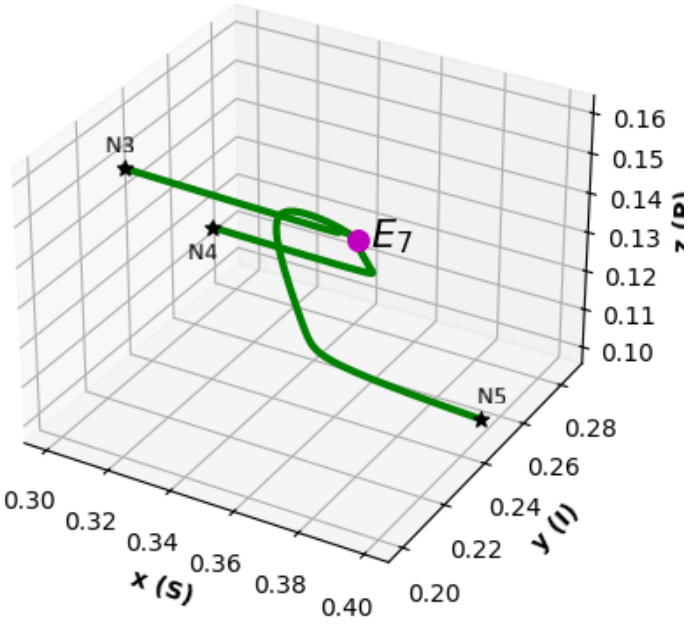

Fig. 2: Convergence to the stable interior equilibrium $E_7(0.385, 0.212, 0.159)$ under Case 2 parameters.

3.3.3. Bistability (Case 3)

For the parameter set in Case 3, the system exhibits bistability. Maple computations reveal two locally asymptotically stable equilibria: the predator-free endemic equilibrium $E_3 = (0.100, 0.492, 0)$ with eigenvalues -1.222, -0.312, and -0.314, and the predator–prey equilibrium without infection $E_6 = (0.336, 0, 7.147)$ with eigenvalues -3.963, -0.563, and -7.674.

In contrast, the interior equilibrium

$$E_7 = (0.296, 0.296, 0.103)$$

is unstable due to the presence of a positive eigenvalue (0.140). Fig. 3 demonstrates that initial conditions $N_7(0.2, 2.1, 0.3)$ and $N_8(0.5, 0.8, 0.05)$ converge to E_3, while $N_6(1.0, 3.5, 8.1)$ and $N_9(1.2, 0.05, 0.1)$ converge to E_6. This behavior indicates the existence of multiple attractors and indicates the existence of a separatrix dividing the basins of attraction. Consequently, long-term ecological outcomes depend crucially on initial population densities under high pesticide pressure.

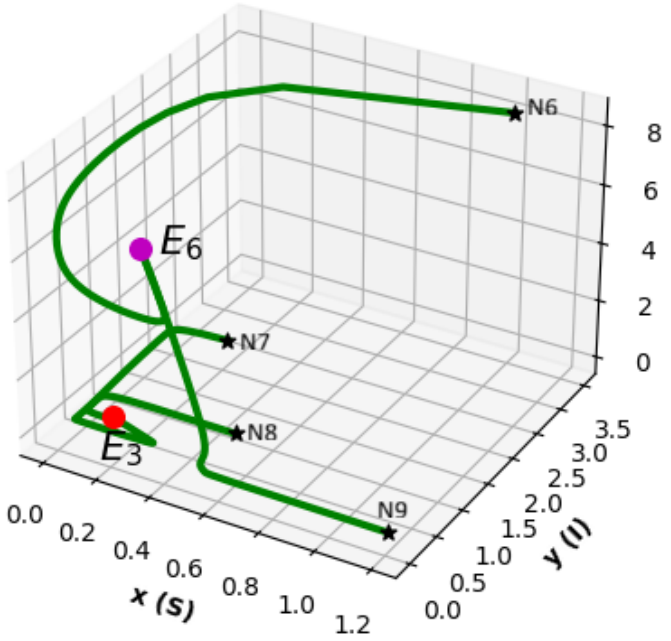

Fig. 3: Bistability between $E_3(0.100, 0.492, 0)$ and $E_6(0.336, 0, 7.147)$ under Case 3 parameters.

3.4. Bifurcation Analysis

The bifurcation diagrams were generated numerically by computing equilibrium branches and tracking their stability through eigenvalue analysis as the bifurcation parameter varies. All other parameters were held fixed at the values specified in the figure captions to ensure reproducibility.

Fig. 4 illustrates the bifurcation structure with respect to the disease transmission rate β, with fixed parameters $r = 9.7$, $K = 0.64$, $u = 0.5$, $h = 2.1$, $\rho = 0.047$, $\alpha = 0.2$, $m = 0.4$, $n = 1.1$, $\mu = 0.063$, and $\eta = 0.26263$ (corresponding to Case 2 parameters). Three bifurcation points are detected: BP_1 at $\beta \approx 0.4$ on the predator-free equilibrium E_3, BP_2 at $\beta \approx 0.6$ on the disease-free equilibrium E_2, and BP_3 at $\beta \approx 22$ on the predator-free equilibrium E_3.

Changes in stability occur at these critical values. At BP_1 ($\beta \approx 0.4$), as β increases through the critical value, one real eigenvalue of the Jacobian evaluated at E_3 crosses from negative to positive, while the corresponding eigenvalue of E_2 crosses from positive to negative. This exchange of stability between two equilibrium branches is characteristic of a transcritical bifurcation.

Biologically, increasing β intensifies infection pressure on the prey population, indirectly influencing predator persistence through reduced prey availability. For $\beta < 0.4$, the predator-free equilibrium E_3 is locally asymptotically stable. When $0.4 < \beta < 0.6$, E_3 loses stability and the disease-free equilibrium E_2 becomes stable. For $0.6 < \beta < 22$, the interior equilibrium E_7 is stable, indicating long-term coexistence of susceptible prey, infected prey, and predators. For sufficiently large transmission rates ($\beta > 22$), the predator-free equilibrium E_3 regains stability at BP_3, suggesting that extreme disease pressure may again inhibit predator persistence.

Fig. 5 presents the bifurcation diagram with respect to the predator conversion coefficient η, with fixed parameters $r = 9.7$, $K = 0.64$, $u = 0.5$, $h = 2.1$, $\rho = 0.047$, $\alpha = 0.2$, $m = 0.4$, $n = 1.1$, $\mu = 0.063$, and $\beta = 0.7$. Two bifurcation points are identified: BP_1 at $\eta \approx 0.077$ on the disease-free equilibrium E_2 and BP_2 at $\eta \approx 21.670$ on the predator-free equilibrium E_3.

At BP_1 ($\eta \approx 0.077$), a transcritical bifurcation occurs as an eigenvalue of E_2 crosses zero, leading to an exchange of stability with E_3. At BP_2 ($\eta \approx 21.670$), another transcritical bifurcation transfers stability from E_3 to the interior equilibrium E_7.

Distinct stability regimes emerge as η varies. For $\eta < 0.077$, the disease-free equilibrium E_2 is stable. When $0.077 < \eta < 21.670$, E_2 loses stability and the predator-free equilibrium E_3

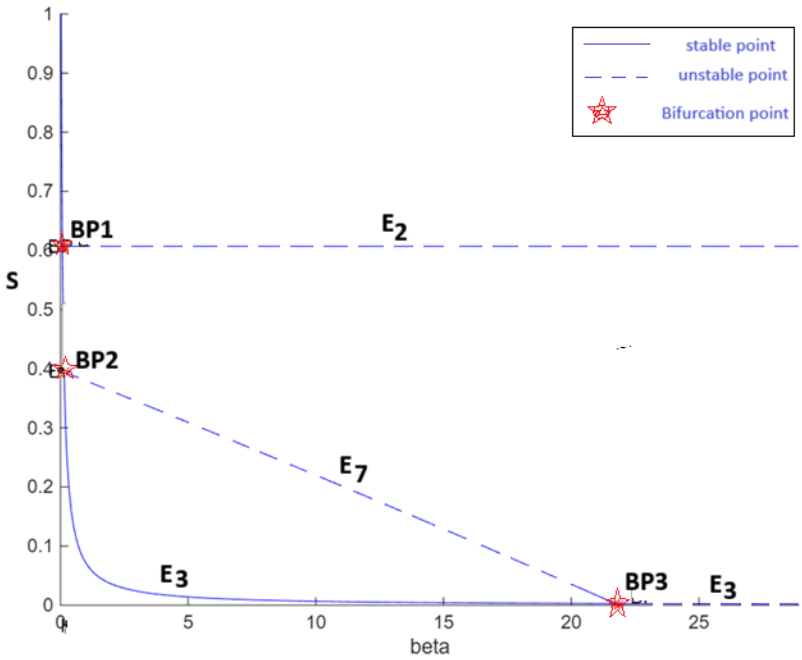

Fig. 4: Bifurcation diagram with respect to β. Fixed parameters: $r = 9.7$, $K = 0.64$, $u = 0.5$, $h = 2.1$, $\rho = 0.047$, $\alpha = 0.2$, $m = 0.4$, $n = 1.1$, $\mu = 0.063$, $\eta = 0.26263$. Solid curves denote stable equilibria, while dashed curves denote unstable equilibria.

becomes stable. Once $\eta > 21.670$, E_3 becomes unstable and the interior equilibrium E_7 gains stability. This indicates that predator persistence requires the conversion coefficient to exceed a critical threshold.

It is important to note the different scales of η used in the bifurcation analysis and the time-series simulations. The bifurcation diagram reveals a theoretical threshold for predator persistence at a high value of $\eta \approx 21.67$. However, in ecologically realistic scenarios, conversion efficiencies are often much lower. To illustrate the system's dynamics within a more plausible range, we selected smaller values of η (e.g., 0.26263 and 3.26263) for the phase portraits in Fig. 1–Fig. 3. These values are well below the main bifurcation threshold and allow demonstration of system behavior under moderate predator efficiency, complementing the mathematical insight gained from the bifurcation structure.

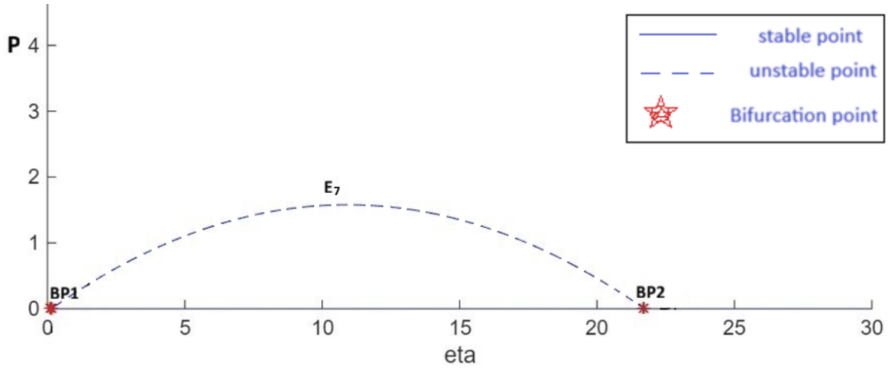

Fig. 5: Bifurcation diagram with respect to η. Fixed parameters: $r = 9.7$, $K = 0.64$, $u = 0.5$, $h = 2.1$, $\rho = 0.047$, $\alpha = 0.2$, $m = 0.4$, $n = 1.1$, $\mu = 0.063$, $\beta = 0.7$. Solid curves denote stable equilibria, while dashed curves denote unstable equilibria.

Overall, the bifurcation analysis reveals critical thresholds governing predator invasion and disease establishment. The bifurcation near $\beta \approx 0.4$ marks a transition in stability between

predator-free and disease-free equilibria, highlighting the sensitivity of predator persistence to disease transmission intensity. Similarly, the threshold $\eta \approx 21.670$ represents the minimum conversion efficiency required for predator survival under strong disease pressure.

These results provide qualitative insight for integrated pest management strategies. Reducing β below critical levels may suppress disease-induced regime shifts, whereas ensuring sufficiently large predator conversion efficiency promotes stable coexistence. The analysis underscores the ecological importance of energy transfer efficiency, since inadequate conversion from prey to predator biomass may prevent predator persistence even when prey populations remain available.

4. Conclusion

This study developed and analyzed an eco–epidemiological predator–prey model that incorporates saturated disease transmission, a Holling type II functional response, and pesticide application acting on the susceptible prey population. Analytical results established the existence and local stability conditions of the trivial, disease-free, predator-free, predator–prey, and interior coexistence equilibria. Local stability was characterized using Jacobian analysis and the Routh–Hurwitz criteria, providing a mathematically consistent description of the system dynamics.

Numerical simulations corroborated the analytical results and revealed multiple dynamical regimes, including stable coexistence, predator extinction, and bistability. In particular, bistability between predator-free and coexistence equilibria implies that long-term ecological outcomes may depend sensitively on initial population densities, even under identical parameter values. This highlights the importance of transient dynamics and initial ecosystem conditions in eco–epidemiological systems.

Bifurcation analysis with respect to key parameters, namely the disease transmission rate β and the predator conversion coefficient η, identified critical thresholds at which stability exchanges occur between equilibria. These thresholds delineate transitions between disease-free states, predator-free states, and full coexistence, and clarify how variations in infection pressure and predator efficiency can qualitatively alter system behavior.

From an ecological management perspective, the results provide *qualitative, model-based insights* relevant to integrated pest management (IPM). In particular, the existence of critical thresholds associated with key epidemiological and ecological parameters, such as the disease transmission rate β and predator conversion efficiency η, suggests that management strategies must carefully balance these factors to avoid pushing the system into an undesirable predator-free state. While the pesticide application rate u is a crucial control parameter, its specific threshold values were not explored in detail here and remain a subject for future investigation.

Several limitations should be noted. Pesticide action is assumed to affect only the susceptible prey class, and non-target effects, economic considerations, and optimal control strategies are not included. Consequently, IPM-related implications should be understood as qualitative guidance derived from the mathematical structure of the model rather than direct management recommendations. Future work may extend the present framework by incorporating time delays, spatial diffusion, non-target pesticide effects, and optimal control formulations to obtain more comprehensive and practically oriented ecological insights.

CRediT Authorship Contribution Statement

Aqiilah Ollyana Savitri: Conceptualization, Methodology, Writing–Original Draft, Visualization, Writing–Review & Editing. **Dian Savitri:** Data Curation, Formal Analysis, Project Administration, Validation.

Declaration of Generative AI and AI-assisted technologies

No generative AI or AI-assisted technologies were used during the preparation of this manuscript.

Declaration of Competing Interest

The authors declare no competing interests.

Funding and Acknowledgments

This research received no external funding.

Data and Code Availability

Code analyzed during the current study are publicly available in the google colab https://colab.research.google.com/drive/1L6O07tXVlBQxlJiLnT_I6422GGbWSknd?usp=sharing.

References

[1] R. Babu and I. A. Wani, "Dynamics of interaction of one prey and two competing predators with population heterogeneity," *Indonesian Journal of Mathematics and Applications*, vol. 2, no. 2, pp. 78–88, 2024. DOI: 10.21776/ub.ijma.2024.002.02.2.

[2] D. N. Prabhumani, M. Shanmugam, S. P. Manickasundaram, and N. G. Thangaraj, "Dynamics of an eco-epidemiological model with infected prey in fractional order," *Mathematical Modelling and Control*, vol. 5, no. 3, pp. 292–304, 2025. DOI: 10.3934/mmc.2025020.

[3] T. Gaber, R. Herdiana, and Widowati, "Dynamical analysis of an eco-epidemiological model experiencing the crowding effect of infected prey," *Communications in Mathematical Biology and Neuroscience*, vol. 2024, no. 3, 2024. DOI: 10.28919/cmbn/8353.

[4] K. Akshaya, S. Muthukumar, M. Siva Pradeep, T. Nandha Gopal, and N. P. Deepak, "Analysis of diseased one prey two predator model with holling type ii functional response," *Telematique*, vol. 24, no. 1, pp. 150–161, 2025.

[5] I. Domínguez-Alemán, I. Domínguez-Alemán, J. C. Hernández-Gómez, and F. J. Ariza-Hernández, "A predator-prey fractional model with disease in the prey species," *Mathematical Biosciences and Engineering*, vol. 21, no. 3, pp. 3713–3741, 2024. DOI: 10.3934/mbe.2024164.

[6] W. W. Mohammed et al., "Stochastic predator–prey interactions with disease dynamics: Fixed point and numerical investigations," *Boundary Value Problems*, 2025. DOI: 10.1186/s13661-025-02159-8.

[7] R. Das and S. K. Sasmal, "Fear induced coexistence in eco-epidemiological systems with infected prey," *Mathematical Biosciences and Engineering*, vol. 22, no. 11, pp. 2897–2922, 2025. DOI: 10.3934/mbe.2025107.

[8] K. Sarkar and S. Khajanchi, "An eco-epidemiological model with the impact of fear," *Chaos: An Interdisciplinary Journal of Nonlinear Science*, vol. 32, p. 083 126, 2022. DOI: 10.1063/5.0099584.

[9] M. S. Rahman, S. Pramanik, and E. Venturino, "An ecoepidemic model with healthy prey herding and infected prey drifting away," *Nonlinear Analysis: Modelling and Control*, vol. 28, no. 2, pp. 326–364, 2023. DOI: 10.15388/namc.2023.28.31549.

[10] Y. Enatsu, J. Roy, and M. Banerjee, "Hunting cooperation in a prey–predator model with maturation delay," *Journal of Biological Dynamics*, vol. 18, no. 1, p. 2 332 279, 2024. DOI: 10.1080/17513758.2024.2332279.

[11] A. H. Naser and D. K. Bahlool, "Modeling disease dynamics in a prey–predator system with competition, fear, and cooperative hunting," *Computation*, vol. 13, no. 11, p. 254, 2025. DOI: 10.3390/computation13110254.

[12] B. Kumar, R. K. Sinha, and S. Hussain, "Comparative analysis of eco-epidemic model with disease in prey and gestation delay in predator: Implications for population dynamics," *Advances in Continuous and Discrete Models*, 2025. DOI: 10.1186/s13662-025-03863-6.

[13] M. K. Dewi, D. Savitri, and Abadi, "Dynamical behavior in the competitive model incorporating the fear effect of prey due to allelopathy with shared biotic resources," *BAREKENG: Journal of Mathematics and Its Applications*, vol. 18, no. 4, pp. 2663–2674, 2024. DOI: 10.30598/barekengvol18iss4pp2663-2674.

[14] K. G. Mekonen, K. P. Rao, and A. F. Bezabih, "Mathematical modeling of infectious disease and prey-predator interaction with optimal control," *International Journal of Mathematics and Mathematical Sciences*, vol. 2024, p. 5 444 627, 2024. DOI: 10.1155/2024/5444627.

[15] H. Qiu, T. Zhang, and R. Hou, "Optimal control of an infected prey–predator model with fear effect," *Nonlinear Analysis: Modelling and Control*, vol. 29, no. 4, pp. 670–692, 2024. DOI: 10.15388/namc.2024.29.35236.

[16] W. Qin, Y. Xia, and Y. Yang, "An eco-epidemic model for assessing the application of integrated pest management strategies," *Mathematical Biosciences and Engineering*, vol. 20, no. 9, pp. 16 506–16 527, 2023. DOI: 10.3934/mbe.2023736.

[17] T. Herlambang, D. Rahmalia, N. Aini, and D. F. Karya, "Predator-prey dynamical model with infected prey by virus and its optimal control using pesticide," in *AIP Conference Proceedings*, vol. 2577, 2022.

[18] K. Mu'tamar, J. Naiborhu, R. Saragih, and D. Handayani, "Nonlinear tracking control for prey stabilization in predator-prey model using backstepping," *BAREKENG: Journal of Mathematics and Its Applications*, vol. 19, no. 3, pp. 1825–1840, 2025. DOI: 10.30598/barekengvol19iss3pp1825-1840.

[19] R. Du, X. Liang, Y. Na, and F. Xu, "Optimal control of an eco-epidemiological reaction-diffusion model," *Mathematics*, vol. 13, no. 13, p. 2069, 2025. DOI: 10.3390/math13132069.

[20] L. Li and J.-E. Zhang, "Input-to-state stability of stochastic nonlinear system with delayed impulses," *Mathematical Biosciences and Engineering*, vol. 21, no. 2, pp. 2233–2253, 2024. DOI: 10.3934/mbe.2024098.

[21] J. G. Clapp, J. L. Malmberg, and J. D. Holbrook, "Examining pathogen avoidance in predator-prey and scavenging systems," *Frontiers in Ecology and Evolution*, vol. 12, p. 1 481 290, 2024. DOI: 10.3389/fevo.2024.1481290.

[22] R. Sivakumar and S. Vijaya, "Eco-epidemiology of prey and competitive predator species in the sei model," *The Scientific Temper*, vol. 15, no. spl-2, pp. 243–252, 2024. DOI: 10.58414/SCIENTIFICTEMPER.2024.15.spl-2.37. https://scientifictemper.com/.

[23] A. A. Raezah, J. Chowdhury, and F. A. Basir, "Global stability of the interior equilibrium and the stability of hopf bifurcating limit cycle in a model for crop pest control," *AIMS Mathematics*, vol. 9, no. 9, pp. 24 229–24 246, 2024. DOI: 10.3934/math.20241179.

[24] N. P. Deepak, S. Muthukumar, M. Siva Pradeep, and T. Nandha Gopal, "Stability analysis of fractional order holling type ii prey predator model with diseased prey," in *AIP Conference Proceedings*, vol. 3122, 2024, p. 040 003. DOI: 10.1063/5.0216020.

[25] D. N. Prabhumani, M. Shanmugam, S. P. Manickasundaram, and N. G. Thangaraj, "Dynamical analysis of a fractional order prey-predator model in crowley-martin functional response with prey harvesting," *Engineering Proceedings*, vol. 56, p. 300, 2023. DOI: 10.3390/ASEC2023-15975.